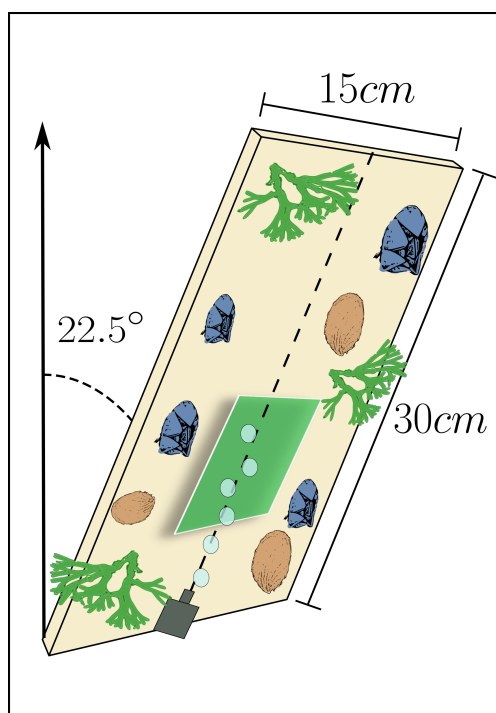


# Using aeration to probe the flow characteristics associated with long-term marine macrofouling growth and suppression



# Using aeration to probe the flow characteristics associated with long-term marine macrofouling growth and suppression

Lena Dubitsky<sup>1</sup>, Mark Menesses<sup>1</sup>, Jesse Belden<sup>2</sup>, and James C. Bird<sup>1\*</sup>

<sup>1</sup>*Department of Mechanical Engineering, Boston University, Boston, MA, USA*

<sup>2</sup>*Naval Undersea Warfare Center, Division Newport, Newport, RI, USA*

Received 28 January 2021; accepted 3 March 2021

## Abstract

It is well-established that hydrodynamics affect the settlement of biofouling organisms. Laboratory studies have demonstrated a connection between larval attachment rates and the prevalence of time windows that satisfy certain instantaneous flow conditions. However, it is unclear whether a link exists between short-term hydrodynamics and long-term macrofouling survival and growth, or if it is applicable at an ecosystem-wide level. This study uses single bubble stream aeration in field and laboratory experiments to find critical flow characteristics that correlate to long-term, multi-species fouling prevention. The research was accomplished by combining PIV-derived flow statistics with fouling severity measured over seven weeks in the field. Flows with a decreasing proportion of time windows defined by a flow speed less than 15.1 mm/s for longer than 0.03 s correlated to decreased biofouling growth and survival. These results provide a potential framework for studying and comparing flow fields that successfully inhibit biofouling growth.

**Keywords:** Aeration; flow characteristics; bubble; macrofouling; grooming

## Introduction

Hydrodynamics has long been recognized as a key factor influencing the biofouling process and plays different roles in each stage of fouling. Ocean currents transport largely passive planktonic larvae until they reach a solid surface[6, 13]. From there, hydrodynamic conditions near the surface affect the behavior of the larvae as they settle and attach[19, 2, 25]. Post-settlement, flow conditions have been shown to alter the growth rates of attached individuals[30, 4]. From larval transport to recruitment, studying how flow fields interact with biofouling organisms is a critical component of understanding and modeling the fouling process.

More recently, studies focused on hydrodynam-

ics have found that instantaneous flow properties—as opposed to mean flow properties—more accurately model observed larval settlement patterns[12, 8]. For a larva near a surface, it only interacts with the localized hydrodynamic conditions. The present study builds on past statistical frameworks for analyzing instantaneous flow properties to examine if macrofouling growth and survival can be understood in terms of instantaneous, local flow characteristics. The study analyzed the hydrodynamic conditions generated by aeration that correlated to long-term, multi-species biofouling prevention in the field.

---

\*[jbird@bu.edu](mailto:jbird@bu.edu)

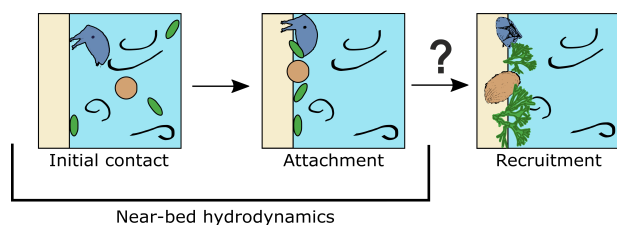


Figure 1: Schematic of the biofouling process. Near-bed hydrodynamics have been studied in the context of settlement. However, it is unclear whether hydrodynamic conditions are important for the recruitment stage or if these ideas can be applied at an ecosystem-wide level, rather than only species-specific.

The biofouling process can be categorized into three broad stages, as shown in Figure 1. Initial contact refers to larval transfer from the water column to the solid surface. Attachment occurs as the organisms explore the surface for suitability and then attach, usually using adhesion. Initial contact and attachment are two stages in the settlement process, while the recruitment stage takes place over weeks and months, as the organisms survive and metamorphose into juveniles and adults [1, 16]. Near-surface, or near-bed hydrodynamics are known to be a crucial factor for the contact and attachment stages for a wide range of biofouling organisms. The responses of larval settlement to changes in flow fields are highly species-specific [18, 15]. This range of responses is thought to be due to larval behavior, which becomes a determining factor in settlement once the larvae reach a surface [10, 23, 24, 26, 14]. Indeed, the settlement rates of planktonic larvae can vary by an order of magnitude due to the effects of larval behavior [11].

It was once assumed that hydrodynamics limited larval settlement by creating lift and drag forces that exceeded the adhesion strength of a larva on a surface [18]. However, more recent studies complicate this picture: it has been documented that barnacle larvae reject flows that have forces far below what they can withstand [21, 20]. In Larsson and Jonsson (2006), it was shown that these flows crossed a threshold where post-settlement survival decreased, meaning that the larvae may prefer hydrodynamic conditions that are most beneficial for the adult stage of the life cycle.

Mean flow velocities in areas where biofouling occurs can be quite low, but instantaneous stresses and velocities can be much higher due to waves, boat wakes, and wind chop [18]. Only recently have biofouling studies started to look at flows other than unidirectional flume flows [17, 28].

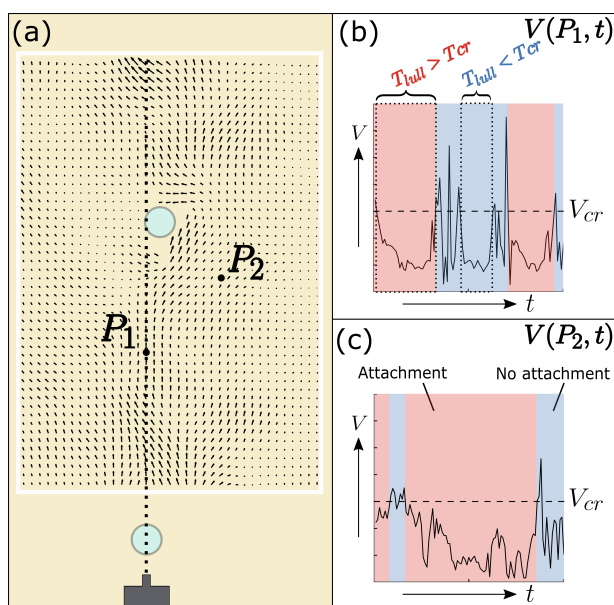


Figure 2: The mechanism by which near-bed hydrodynamics affect biofouling settlement, as outlined in Crimaldi (2002). (a) An instantaneous flow field showing the velocity 0.4 mm from the surface. Two different points in the flow field,  $P_1$  and  $P_2$ , are highlighted. (b) A plot of velocity magnitude over time at centerline location  $P_1$ . When a larva encounters a surface, it experiences the fluctuations of the near-bed velocity. A fouling organism can only attach to a surface when the local flow velocity is below a critical velocity,  $V_{cr}$ , for a period of time longer than the critical time,  $T_{cr}$ . A time window that satisfies these two conditions is defined as a settling window,  $T_{sw}$ . A lull period,  $T_{lull}$ , occurs whenever the velocity falls below  $V_{cr}$ . (c) A plot of the velocity magnitude over time at location  $P_2$ . Settling windows, when attachment is possible, are shaded in red, while periods where attachment is not possible are shaded in blue. The proportion of settling windows in a flow indicates the likelihood of fouling occurring there. In this case, location  $P_2$  would be expected to be more fouled than location  $P_1$ .

Crimaldi et al. (2002) introduced the idea of a probability of larval attachment, based on a statistical analysis of turbulent flow that can account for instantaneous hydrodynamic properties. The probability of attachment is based on the proportion of the flow field that, over time, contains suitable time windows that allow for larvae to settle on the surface [8]. Time windows are suitable for settlement when the local flow is below a critical velocity,  $V_{cr}$ , for a sufficient period of time,  $T_{cr}$ . The mechanism is outlined

in Figure 2. Larsson et al. (2016) experimentally calculated the critical velocity and time window for barnacle cyprid larvae and found that  $V_{cr} = 24$  mm/s and  $T_{cr} = 0.1$  s.

The results of Crimaldi et al. (2002) and Larsson et al. (2016) demonstrated that the probability of attachment theory, which analyzes the instantaneous hydrodynamic conditions near the surface, is an important factor determining the settlement of barnacles and clams. However, both previous sets of experiments only examined the larval settlement stage and were conducted in a carefully controlled laboratory environment. It is unclear if the probability of attachment theory is applicable to field conditions or if it is relevant for the recruitment stage of the biofouling process.

The present study aims to adopt the attachment probability analysis and combine it with field data on the growth of multiple species of fouling organisms well beyond the settling period. Aeration, which has been studied as a method of biofouling prevention [29, 5, 22], provides a convenient platform to explore if variations in near-bed hydrodynamics can explain different long-term outcomes for multiple macrofouling species and whether an ecosystem-wide critical velocity and settling time window exist for these flows.

## Materials and methods

### Field experiments

The field experiments took place in Narragansett Bay, Rhode Island, USA in the summer of 2016. The tests lasted for seven weeks through the months of June and July. A field rig was designed to hold five uncoated Garolite G-10 epoxy test panels off a dock edge. The panel depth was at an average of 1.8 m below the water surface, with local tide swings of  $\pm 0.6$  m. The epoxy panels measured 30 cm x 15 cm and were affixed at a  $22.5^\circ$  angle from the vertical, as shown in Figure ??a. The panels were hydrophilic with a measured contact angle of  $73.5^\circ$  [22], and had an elastic modulus of 20GPa[27]. A single air nozzle was located at the bottom of four of the panels and released bubbles at controlled flow rates. Bubbles with a mean equivalent diameter of 5.2 mm were emitted at a different frequency for each panel:  $f = 0.03$  Hz, 0.3 Hz, 3 Hz, and 30 Hz. The fifth panel without a nozzle was left as a control and not aerated. The panels were lifted out of the water and photographed weekly using a Nikon D7000 camera (Nikon, Japan)

in order to track the biofouling growth.

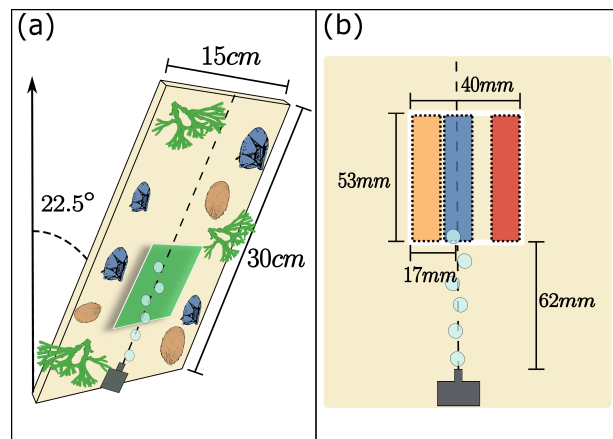


Figure 3: Illustration of the laboratory and field study set-up. (a) Orientation of the panels during the field and laboratory studies. Note the angle offset from vertical, which allowed the bubbles to slide along the surface. The green region indicates where PIV measurements were taken in the laboratory study. Note that the PIV data was taken using an unfouled surface. (b) Dimensions and location of the PIV measurement region. The region was divided into three sections (Left, Center, and Right) that were 2 bubble widths across. PIV data and fouling scores were only considered in these three regions.

### Laboratory measurements

The characteristics of the four bubble flows were measured using Particle Image Velocimetry (PIV). The panel and nozzle setup were installed in a tank filled with tap water, with the nozzle air flow rate adjusted accordingly to replicate each flow case. The water was seeded with  $33 \mu\text{m}$  mean diameter fluorescent polystyrene particles with a density of  $1.19 \text{ g/cm}^3$ . A laser sheet was created using a 532 nm single, continuous, 5 watt laser (Coherent Verdi G5, California, USA). The  $800 \mu\text{m}$ -thick laser sheet was illuminated parallel to the plate, at a distance of 0.4mm from the surface, which is similar to the size of a macrofouling larva[20]. A high-speed camera (Phantom v5, New Jersey, USA) with a 105 mm macro lens recorded 53 mm x 40 mm images at a rate of 300 frames per second, with the entire data set consisting of over 2000 frames. The image resolution was 800 x 600 pixels which was then broken into 16 x 16 pixel interrogation windows and processed using Lavision FlowMaster PIV software (LaVision, Ypsilanti, MI, USA).

## Data analysis

### Biofouling image analysis

Once the photographs of the fouled epoxy plates were obtained, a quantitative measurement of the macro-fouling severity was determined. The images were analyzed only within the area where PIV measurements were taken to facilitate a direct comparison. The PIV measurement area was split into three segments: Left, Center, and Right, with respect to the nozzle centerline. Each segment was two bubble widths across with a height equal to the PIV field of view and was composed of 581 pixels. The Center segment was centered above the nozzle, while the Left and Right segments were flush with each respective edge of the PIV measurement area, as shown in Figure 3b. A large sampling area was chosen to limit the effects of variability on the larval scale and obtain results more characteristic of the extent of fouling that might be established on a large, submerged surface, such as a ship's hull.

To calculate a measure of fouling severity, the images were converted to greyscale and then noise-filtered using the wiener2 function (MATLAB, Mathworks, Natick, MA, USA). On each panel, a 'clean benchmark' pixel value was identified by picking the visually cleanest area within the top third of the panel and sampling pixels within that region. For each of the three segments, the greyscale pixel values were subtracted from the clean benchmark and then averaged ( $P_x$ ). The mean standard deviation (SD) ( $\mu_x$ ) for the segment was also calculated, as demonstrated in Figure 4. A fouling score was constructed using the following equations:

$$F_x = \mu_x P_x \quad (1)$$

$$\hat{F}_x = \frac{F_x}{F_{control}} \quad (2)$$

Where  $F_x$  is the fouling score of segment  $x$  (with  $x$  being Left, Center, or Right),  $\mu_x$  is the mean SD of segment  $x$ ,  $P_x$  is the mean difference in pixel value of the segment from the clean benchmark,  $\hat{F}_x$  is the normalized segment fouling score, and  $F_{control}$  is the fouling score for all three segments of the control panel.

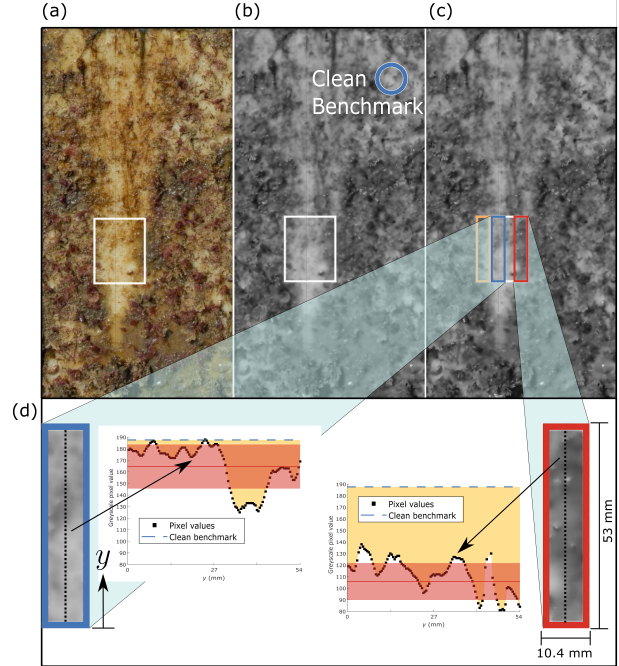


Figure 4: An example of the image processing analysis to obtain fouling scores. (a) A photograph of the  $f = 3$  Hz panel on Week 6, with the PIV measurement region denoted by the white box. (b) The photograph after converting to greyscale and adaptive noise-filtering. The clean benchmark region is shown in the top right. (c) The three analysis regions (Left, Center, Right) outlined in orange, blue, and red, respectively. (d) Expanded view of the Center and Left regions. The centerline pixel values are sampled (shown as the dotted line), along with the pixel value of the clean benchmark. The difference between the pixel values and the clean benchmark is shown in yellow ( $P_x$ ). The SD of the measured pixel values is shown in red ( $\mu_x$ ). The mean difference and mean SD for the entire region are multiplied to obtain a fouling score. That score is then normalized by the same calculation done for the control panel.

### Flow statistics analysis

The PIV velocity data were analyzed for lull periods and settling windows using a custom MATLAB script. Settling windows are defined by a critical velocity,  $V_{cr}$ , and critical time window,  $T_{cr}$ . Both of these variables are unknown in the study, so settling windows were calculated for a range of both.  $V_{cr}$  was varied between 0 and 150 mm/s, while the  $T_{cr}$  values used were 0.003, 0.01, 0.03, 0.05, 0.1, 0.3, 0.5, 1, and 3 seconds. The range of critical velocity values was

chosen to encompass the highest velocities measured within the PIV data. The critical time window values include the time step between data collection points, the periods of bubbling frequencies, and the length of the data collection period (3 s). Each spatial PIV data point within the segments (Left, Center, Right) was analyzed for settling windows and lull periods over the entire PIV data collection period, as illustrated in Figure 2b and c.

The probability of attachment,  $P_A$ , is the proportion of time over which the flow remains below the critical velocity  $V_{cr}$  for a duration that exceeds  $T_{cr}$ . The cumulative probability of attachment  $P_A$  for a given  $V_{cr}$  and  $T_{cr}$  is found by the following formula, following Larsson et al. (2016)[20]:

$$P_A(V_{cr}, T_{cr}) = \frac{\sum_{i=1}^N T_{sw,i}(V_{cr}, T_{cr}) - N * T_{cr}}{T} \quad (3)$$

Where  $T_{sw}$  is the settling window length,  $N$  is the number of identified settling windows and  $T$  is the total time represented in the data set.

## Results

### Field results

The results of the seven-week field study are depicted in Figure 5. Starting with clean surfaces on the left of the figure, fouling accumulated on the plates, accelerating in Weeks 5, 6, and 7. There were clean wedge-shaped regions in areas where bubbles passed by, demonstrating the prevention of biofouling growth. On panels exposed to decreasing bubbling frequencies, this wedge shape became thinner and shorter. In weeks 6 and 7 of the  $f = 30$  Hz case, brown algae grew over the previously clean region. However, it remained free of macrofoulers such as barnacles and clams. In all other flow cases, macrofoulers became apparent in weeks 6 and 7.

Fouling scores were computed using Eqs. 1 and 2 for the Week 6 data set, which corresponded to when macrofouling organisms were growing on the plates but before brown algae obscured the signal from the previously clean region. Fouling scores for the three PIV segments (Left, Center, Right) for each flow case are reported in Table 1. Note that there are values reported greater than one, which indicates that the panel segment was more fouled than the control.

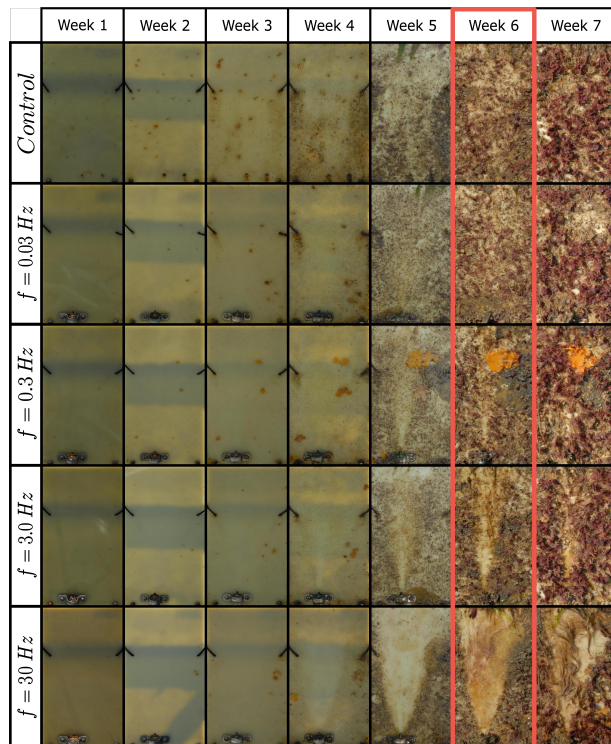


Figure 5: A compilation of the field test results, shown for each panel across 7 weeks of the study. The row labels indicate the frequency of bubbles emitted from the nozzle. All data analysis was done on Week 6 results.

|               | Left | Center | Right |
|---------------|------|--------|-------|
| $f = 0.03$ Hz | 0.98 | 0.95   | 0.98  |
| $f = 0.3$ Hz  | 1.22 | 0.87   | 1.23  |
| $f = 3$ Hz    | 0.57 | 0.17   | 0.84  |
| $f = 30$ Hz   | 0.22 | 0.22   | 0.23  |

Table 1: Week 6 Fouling Scores

The colors in Table 1 correspond to the fouling score - the darker the color, the higher the fouling score. From this color scheme it is apparent that as the bubbling frequency increased, the Center segment became dramatically less fouled. However, the Left and Right segments also became somewhat cleaner due to the bubbles meandering and spreading out over the submerged panel. Once the frequency reached 30 Hz, the clean region spanned all three segments. These results are consistent with previous single bubble aeration experiments done in Narragansett Bay, where a bubble frequency of 24 Hz largely prevented macrofouling growth over the course of 7 weeks[22].

## Laboratory results

The PIV data were analyzed to identify settling windows (where  $V < V_{cr}$  and  $T > T_{cr}$ ) and lull windows (where  $V < V_{cr}$ ) in the four bubbling flow conditions. Mean probabilities of attachment were computed for each segment of each flow condition using Equation 3. As shown in Figure 6, a probability curve consists of the attachment probability computed for one  $T_{cr}$  value, over the full range of critical velocity values. A different  $T_{cr}$  results in an alternate set of curves, as shown in the figure for  $T_{cr} = 0.5$  s. As the bubbling frequency increases the attachment probability, or the proportion of the flow that contains settling windows, decreases.

In order to find values for  $V_{cr}$  and  $T_{cr}$ , a least-squares regression analysis was used to fit the fouling scores of the Left, Center, and Right segments to the probabilities of attachment for those corresponding segments. This method allows for a connection between the instantaneous PIV flow measurements and the long-term fouling data. The probability curves and the line of best fit along the fouling scores are plotted in Figure 6. The best fit resulted in a critical time window,  $T_{cr}$ , of 0.03 s and critical velocity,  $V_{cr}$ , of 15.1 mm/s. For these values the attachment probability is below 0.1 for the highest bubbling frequency flow case, and between 0.8-1 for the lowest frequency, which broadly follows with the fouling score values.

## Discussion

This investigation aimed to determine whether near-bed hydrodynamics can be used to understand the different levels of macrofouling documented over the course of a 7-week field study in Narragansett Bay, Rhode Island. The methods described here may be a novel technique of analyzing and understanding flow fields that prevent long-term macrofouling growth. Using bubble streams with increasing frequencies allowed for insight into the time-varying nature of the flow fields. In contrast to flume flow studies, where an increase in velocity corresponds to an increase in turbulence, the use of bubbles allows for some control over the time periods between turbulent events caused by the passing of a bubble. The difference in bubble frequencies led to considerable macrofouling prevention, as captured in the fouling score measure. The PIV data documented the time-varying component of the flow which was analyzed in terms of the attachment probability. Combining the field and laboratory measurements resulted in a critical time win-

dow and critical velocity that describe the threshold for fouling prevention at the ecosystem level.

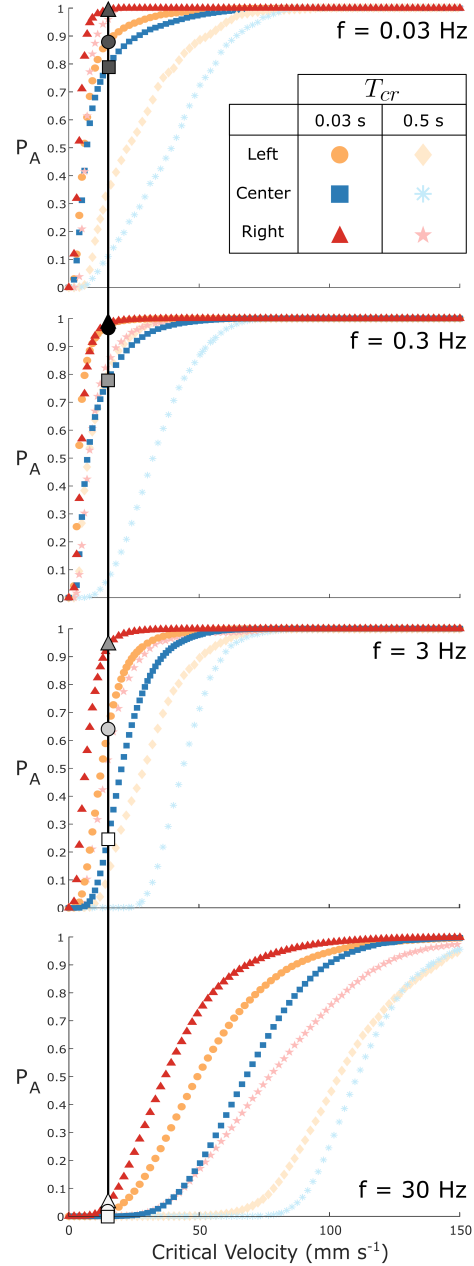


Figure 6: Probability of attachment curves calculated for the three regions (Left, Center, Right), for all four flow conditions with a critical time window  $T_{cr} = 0.03$  s and  $T_{cr} = 0.5$  s. The vertical line indicates the line of best fit, at  $V_{cr} = 15.1$  mm/s. This result was found by fitting the fouling scores from Table 1 to the probability of attachment data using a least squares regression analysis.

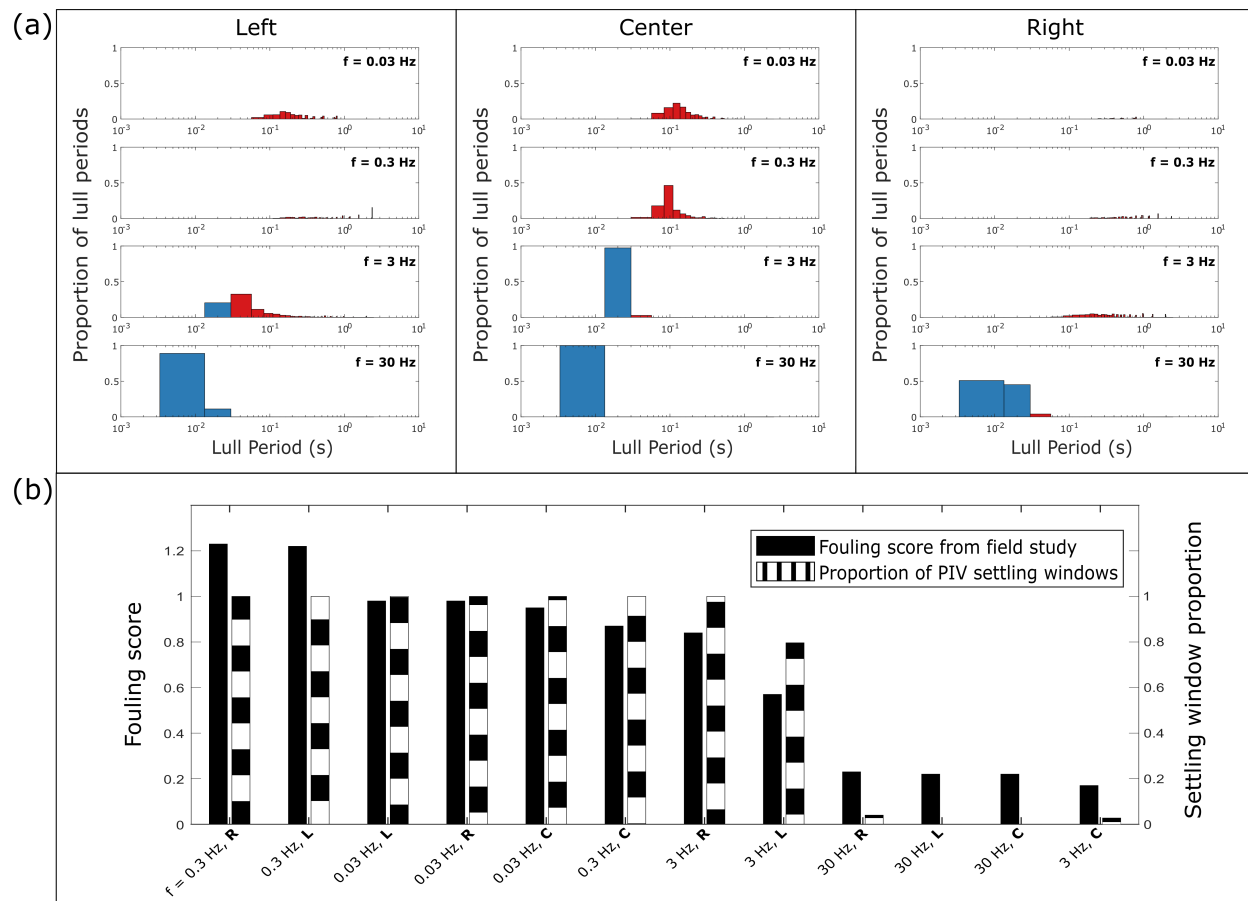


Figure 7: Analysis of identified lull periods with the best-fit critical velocity  $V_{cr} = 15.1$  mm/s. a) Histograms for the Left, Center, and Right regions showing all identified mean lull periods,  $T_{lull}$ , (where  $V < V_{cr}$  for any length of time) for the four flow conditions. The blue histogram bars indicate the proportion of grid points on the plate that have a mean lull period shorter than the critical settling window time,  $T_{cr} = 0.03$  s. Red bars indicate settling windows,  $T_{sw}$ , where the  $T_{lull} > T_{cr}$ . b) Fouling scores plotted from highest to lowest along with the corresponding proportion of settling windows in the flow. The settling window proportion is the sum of red bars in the histogram. As the proportion of settling windows decreases, there is a sharp decrease in fouling score. A correlation analysis between the two data sets results in a  $\rho$ -value of 0.87 and a p-value of 2E-4.

Once a critical time window and velocity were established, it was possible to further investigate the characteristics of the flow fields. In addition to identifying all of the settling windows for each  $V_{cr}$  and  $T_{cr}$ , the lull periods for each  $V_{cr}$  were also recorded, regardless of their length. Figure 7a displays histograms of the lull periods recorded in the Left, Center, and Right regions for the best fit of  $V_{cr} = 15.1$  mm/s. The mean lull period was found for each grid point of the PIV data set for the full time history. To test how well the fitted  $V_{cr}$  and  $T_{cr}$  correlate with long-term fouling outcomes, the fouling scores were

organized from highest to lowest for the 12 regions (Left, Center, and Right for four flow conditions). For each segment, the proportion of the PIV time history that was made up of settling windows (lull periods that were greater than  $T_{cr}$ ), were organized in the same order as the fouling scores as shown in Figure 7b.

|                                   | $\rho$ | p-value |
|-----------------------------------|--------|---------|
| Fouling score to settling window  | 0.87   | 2.0E-4  |
| Fouling score to zero lull period | 0.79   | 2.4E-3  |

Table 2: Correlation analysis

A Spearman's  $\rho$  correlation analysis was performed on the two data sets in Figure 7b using a statistical significance level  $\alpha$  of 0.05. The analysis, summarized in Table 2, found a  $\rho$ -value of 0.87 and a p-value of 2E-4. A similar analysis to test the correlation between the value of the fouling scores and the probability of a point on the plate having no lull periods found a  $\rho$ -value of 0.79 and a p-value of 2.4E-3. A flow with no lull periods would indicate that the velocity was always greater than the critical velocity,  $V_{cr}$ . In other words, the correlation between fouling severity and the prevalence of lull periods greater than  $T_{cr}$  is stronger than the correlation between fouling severity and the flow not having any lull periods at all. The fluctuating component of the flow seems to be quite important in affecting macrofouling settlement and growth.

A separate question is mechanism by which aeration affects the biofouling process. Antifouling mechanisms can generally be categorized as prevention or removal strategies. Antifouling coatings prevent biofouling growth by creating an inhospitable environment for settlement[7]. Removal strategies consist of periodic grooming to detach any organisms that have already settled[31, 32]. In the case of aeration, it is possible that the stream of passing bubbles dislodges newly settled larvae, or that the fluctuations caused by the bubbles remove any opportunity for settlement. The best-fit critical time window is on the same timescales as the initial contact and attachment stages. Furthermore, the duration of this time window is similar to the one previously found for larval settlement by Larsson et al. (2016). Therefore, it is plausible that the high-frequency bubble streams prevent biofouling by disrupting the settling process, consistent with the settling window theory.

There are several potential mechanisms to explain this disruption of the settling process. Barnacle cyprid larvae seem to reject flow conditions even when they can withstand the hydrodynamic forces, due to future detrimental effects on the juvenile barnacles once they metamorphose[21]. In Larsson et al. (2016), it was thought that the critical velocity represented how quickly cyprids can swim against the flow so that they are able to remain stationary relative to the surface in order to attach. For larvae that are not as strong of swimmers, there may be different prevention mechanisms at play. It may also be that bubbles prevent settlement by scavenging larvae out of the water column near the surface, as it has been noted that several larval species appear to be hydrophobic and are easily dewetted onto air-water

interfaces[9, 3]. However, it is unlikely that bubble scavenging is a dominant mechanism overall, as previous studies have found similar levels of macrofouling prevention when comparing panels aerated by bubbles to panels exposed to a jet of water[22].

Given that previous laboratory flume flow experiments have shown high variation in the settlement response of different macrofouling species[15], it is somewhat surprising that one flow condition is able to prevent a wide range of macrofouling. This existence of an ecosystem-wide critical settling window could be an effect of the biofouling process in the field, if it is the case that biofouling growth depends on the succession of multiple different organisms. It is possible that the ecosystem-wide critical values correspond to the conditions needed to keep a key species off the surface, which discourages subsequent macrofouling growth. Another hypothesis is that the critical values represent the minimum flow conditions required to keep the hardest larval species off the surface, while other species within the ecosystem have lower tolerance thresholds. In this case, it would be expected that within different ecological communities these critical values would change.

In summary, examining a variety of bubbling flow conditions both in the field and in the laboratory allowed for the study of correlations between instantaneous flow characteristics and the prevention of long-term, multi-species macrofouling growth. This approach contrasts with previous studies that have examined the temporary attachment of single larval species. Combining fouling scores with probability-of-attachment curves led to a best fit that indicated an ecosystem-wide critical velocity of 15.1 mm/s, and a critical time window of 0.03 s. Previous studies have found a  $V_{cr}$  and  $T_{cr}$  of 24 mm/s and 0.1 s for barnacle larvae[20]. Although it is not expected that these values would be similar, these results indicate that aeration prevents fouling growth at the settling stage and seems to apply for a wide range of macrofouling species. These results are a first step towards examining the applicability of these threshold values in other biofouling ecosystems around the world. Further experiments would be beneficial to generalize and extend the conclusions drawn here, given the limited sampling and replication of the field experiments. The methods described in this study can be used to test if similar correlations exist between instantaneous flow characteristics and long-term fouling outcomes, as well as mechanistically understand these correlations.

## Acknowledgements

The authors acknowledge J. Rekos and M. Boyer for their assistance with the field campaign, and Dr. F. Brasz for his assistance in PIV data collection.

## Funding

This work was supported by the Office of Naval Research under Grant No. N00014-16-1-3000. M.M acknowledges support by the National Science Foundation Graduate Research Fellowship Program under Grant No. DGE-1247312 and an internship provided through the Graduate Research Internship Program (GRIP). L.D acknowledges support by the National Science Foundation Graduate Research Fellowship Program under Grant No. DGE-1840990. Any opinions, findings, and conclusions or recommendations expressed in this material are those of the authors and do not necessarily reflect the views of the funding agencies.

## References

- [1] Avigdor Abelson and Mark Denny. Settlement of marine organisms in flow. *Annual Review of Ecology and Systematics*, 28(1):317–339, 1997.
- [2] Avigdor Abelson, Daniel Weihs, and Yossi Loya. Hydrodynamic impediments to settlement of marine propagules. and adhesive-filament solutions. *Limnology and Oceanography*, 39(1):164–169, 1994.
- [3] Nick Aldred, Caitlyn M Gatley-Montross, Meredith Lang, Michael R Detty, and Anthony S Clare. Correlative assays of barnacle cyprid behaviour for the laboratory evaluation of antifouling coatings: a study of surface energy components. *Biofouling*, 35(2):159–172, 2019.
- [4] Ángel Borja, Pedro Liria, Iñigo Muxika, and Juan Bald. Relationships between wave exposure and biomass of the goose barnacle (*pollicipes pollicipes*, gmelin, 1790) in the gaztelugatxe marine reserve (basque country, northern spain). *ICES Journal of Marine Science*, 63(4):626–636, 2006.
- [5] Stephan G Bullard, Sandra E Shumway, and Christopher V Davis. The use of aeration as a simple and environmentally sound means to prevent biofouling. *Biofouling*, 26(5):587–593, 2010.
- [6] CA Butman. Larval settlement of soft-sediment invertebrates: the spatial scales of pattern explained by active habitat selection and the emerging role of hydrodynamical processes. *Oceanogr. Mar. Biol*, 25:113–165, 1987.
- [7] Lily D Chambers, Keith R Stokes, Frank C Walsh, and Robert JK Wood. Modern approaches to marine antifouling coatings. *Surface and Coatings Technology*, 201(6):3642–3652, 2006.
- [8] John P Crimaldi, Janet K Thompson, Johanna H Rosman, Ryan J Lowe, and Jeffrey R Koseff. Hydrodynamics of larval settlement: the influence of turbulent stress events at potential recruitment sites. *Limnology and Oceanography*, 47(4):1137–1151, 2002.
- [9] Dennis John Crisp. The behaviour of barnacle cyprids in relation to water movement over a surface. *Journal of Experimental Biology*, 32(3):569–590, 1955.
- [10] DJ Crisp, G Walker, GA Young, and AB Yule. Adhesion and substrate choice in mussels and barnacles. *Journal of Colloid and Interface Science*, 104(1):40–50, 1985.
- [11] James E Eckman, Francisco E Werner, and Thomas F Gross. Modelling some effects of behavior on larval settlement in a turbulent boundary layer. *Deep Sea Research Part II: Topical Studies in Oceanography*, 41(1):185–208, 1994.
- [12] JE Eckman, WB Savidge, and TF Gross. Relationship between duration of cyprid attachment and drag forces associated with detachment of *balanus amphitrite* cyprids. *Marine Biology*, 107(1):111–118, 1990.
- [13] Jon N Havenhand and IB Svane. *Ciona intestinalis*. *Mar. Ecol. Prog. Ser*, 68:271–276, 1991.
- [14] SR Jenkins. Larval habitat selection, not larval supply, determines settlement patterns and adult distribution in two chthamalid barnacles. *Journal of Animal Ecology*, 74(5):893–904, 2005.
- [15] Per R Jonsson, Kent M Berntsson, and Ann I Larsson. Linking larval supply to recruitment: flow-mediated control of initial adhesion of barnacle larvae. *Ecology*, 85(10):2850–2859, 2004.
- [16] Michael J Keough and Barbara J Downes. Recruitment of marine invertebrates: the role of active larval choices and early mortality. *Oecologia*, 54(3):348–352, 1982.
- [17] MAR Koehl, JP Crimaldi, and DE Dombroski. Wind chop and ship wakes determine hydrodynamic stresses on larvae settling on different microhabitats in fouling communities. *Marine Ecology Progress Series*, 479:47–62, 2013.
- [18] MRA Koehl. Mini review: hydrodynamics of larval settlement into fouling communities. *Biofouling*, 23(5):357–368, 2007.
- [19] Jean O Lacoursière. A laboratory study of fluid flow and microhabitat selection by larvae of *simulium vittatum* (diptera: Simuliidae). *Canadian Journal of Zoology*, 70(3):582–596, 1992.
- [20] Ann I Larsson, Lena M Granhag, and Per R Jonsson. Instantaneous flow structures and opportunities for larval settlement: barnacle larvae swim to settle. *PloS one*, 11(7), 2016.

- [21] Ann I Larsson and Per R Jonsson. Barnacle larvae actively select flow environments supporting post-settlement growth and survival. *Ecology*, 87(8):1960–1966, 2006.
- [22] Mark Menesses, Jesse Belden, Natasha Dickenson, and James Bird. Measuring a critical stress for continuous prevention of marine biofouling accumulation with aeration. *Biofouling*, 33(9):703–711, 2017.
- [23] LS Mullineaux and CA Butman. Initial contact, exploration and attachment of barnacle (balanus amphitrite) cyprids settling in flow. *Marine Biology*, 110(1):93–103, 1991.
- [24] LS Mullineaux and ED Garland. Larval recruitment in response to manipulated field flows. *Marine Biology*, 116(4):667–683, 1993.
- [25] Joseph R Pawlik and Cheryl Ann Butman. Settlement of a marine tube worm as a function of current velocity: Interacting effects of hydrodynamics and behavior1. *Limnology and Oceanography*, 38(8):1730–1740, 1993.
- [26] Fabrice Pernet, Réjean Tremblay, and Edwin Bourget. Settlement success, spatial pattern and behavior of mussel larvae mytilus spp. in experimental 'downwelling' systems of varying velocity and turbulence. *Marine Ecology Progress Series*, 260:125–140, 2003.
- [27] K Ravi-Chandar and S Satapathy. Mechanical properties of g-10 glass-epoxy composite. Technical report, TEXAS UNIV AT AUSTIN INST FOR ADVANCED TECHNOLOGY, 2007.
- [28] Matthew A Reidenbach, Jeffrey R Koseff, and MAR Koehl. Hydrodynamic forces on larvae affect their settlement on coral reefs in turbulent, wave-driven flow. *Limnology and oceanography*, 54(1):318–330, 2009.
- [29] AJ Scardino, LE Fletcher, and John Anthony Lewis. Fouling control using air bubble curtains: protection for stationary vessels. *Journal of Marine Engineering & Technology*, 8(1):3–10, 2009.
- [30] FG Walton Smith. Effect of water currents upon the attachment and growth of barnacles. *The Biological Bulletin*, 90(1):51–70, 1946.
- [31] Melissa Tribou and Geoffrey Swain. The use of proactive in-water grooming to improve the performance of ship hull antifouling coatings. *Biofouling*, 26(1):47–56, 2010.
- [32] Melissa Tribou and Geoffrey Swain. Grooming using rotating brushes as a proactive method to control ship hull fouling. *Biofouling*, 31(4):309–319, 2015.